

# 通道间隔可切换的双 Lyot 滤波器的结构设计 与性能分析

忻伶俐<sup>1</sup>, 周雪芳<sup>1\*</sup>, 毕美华<sup>1</sup>, 杨国伟<sup>1</sup>, 胡森<sup>1</sup>, 李浩珍<sup>1</sup>, 王天枢<sup>2</sup>

<sup>1</sup>杭州电子科技大学通信工程学院, 浙江 杭州 310018;

<sup>2</sup>长春理工大学空间光电技术研究所, 吉林 长春 130022

**摘要** 在传输矩阵理论推导与实验验证的基础上, 提出了一种通道间隔可切换的全光纤梳状滤波器。该滤波器基于双 Sagnac 环滤波结构, 是两个 Lyot 滤波器的并联。滤波器的两条支路分别由偏振控制器(PC)和不同长度的保偏光纤(PMF)组成, 可通过调节 PCs, 控制光进入 PMF 时的偏振态, 实现通道间隔切换和消光比调谐。其中, 通道间隔分别由两支路上的 PMFs 特性决定, 通过改变 PMFs 的长度和双折射率, 可得到不同的通道间隔可切换组合。在上述设计的基础上, 增设了一个 PC, 经实验检验, 滤波器的可调性得到了进一步提升。最后, 实验证实了以此滤波器为基础构建的多波长光纤激光器(MWFL)在实现通道间隔切换方面的可行性。

**关键词** 光纤光学; 梳状滤波器; 传输矩阵; Lyot 滤波器; 通道间隔可切换

中图分类号 O436

文献标志码 A

DOI: 10.3788/CJL202249.2106002

## 1 引言

周期性光学滤波器是密集波分复用光网络中不可或缺或波长选择元件。其中, 光纤梳状滤波器因其低廉的成本、简单的结构、较小的插入损耗、较强的稳定性及与光纤通信系统极强的兼容性而受到广泛关注。经典的梳状滤波器有 Sagnac 环形镜<sup>[1-3]</sup>、Lyot 滤波器<sup>[4-6]</sup>、马赫-曾德尔干涉仪<sup>[7-8]</sup>、法布里-珀罗滤波器<sup>[9-10]</sup>、光纤光栅<sup>[11]</sup>、纤芯偏移结构<sup>[12-13]</sup>等, 其他一些特殊的滤波器大多是上述滤波器的改进变形<sup>[14-18]</sup>。通常情况下, 特定的梳状滤波器对应固定的通道间隔。然而, 在一些实际应用中, 单一的通道间隔不能满足可调谐性的要求。

多波长光纤激光器(MWFL)是光纤梳状滤波器的常见应用场景。为了使激光器更实用、操作更灵活, 研究者们对常见的全光结构梳状滤波器进行改进, 取得了一定的成果。Luo 等<sup>[19]</sup>在双通马赫-曾德尔干涉仪的一个臂上增加了偏振控制器(PC), 破坏了光在滤波器中两次干涉的固定数值关系, 构造了通道间隔可切换的滤波器结构。此类滤波器的两种通道间隔由臂长差决定, 灵活性相对较差。为了提高灵活性, 通道间隔依赖于保偏光纤(PMF)双折射率的滤波器成为研究热点。Wang 等<sup>[20]</sup>通过理论分析和实验测试, 设计

了一种基于两段级联 PMFs 的 Sagnac 环滤波装置的 MWFL。该激光器的滤波装置可在特定 PC 旋转角度下, 得到均匀可切换的通道间隔, 但多波长输出不能实现通道间隔切换。Wang 等<sup>[21]</sup>和 Zhao 等<sup>[22]</sup>通过级联 Lyot 滤波器的方式, 先后得到了三种和两种由 PMF 性质决定的、通道间隔可切换的滤波透射谱。研究者以此滤波结构为基础构建的 MWFL 获得了 0.48、0.73、1.45 nm 三种通道间隔可切换的稳定多波长输出。除了级联不同长度的 PMF 外, 还可通过并联 PMF 来构造通道间隔可切换的梳状滤波器。

针对 He 等<sup>[23]</sup>提出的由两段不同长度的 PMF 并联组成的双 Sagnac 环结构在理论研究方面的不足, 本团队对双 Sagnac 环结构进行了详细的理论探究和传输特性测试, 并在实验上证实了其应用于 MWFL 时在通道间隔切换上的可行性<sup>[24]</sup>。在上述工作的基础上, 本文将双 Sagnac 环结构展开, 改造出一种新型的基于并联 PMF 的双 Lyot 滤波器干涉结构, 并理论分析和实验验证了其通道间隔可切换的特性。该结构通过 PMF 产生波长相关相位差, 通过调节 PC 可改变偏振态与 PMF 主轴的夹角, 实现通道间隔切换。通过更换不同的 PMFs, 可以得到更多可切换的通道间隔组合, 结构灵活性较强。基于该滤波器设计的 MWFL, 可通过调节 PC, 实现两种不同通道间隔的多波长输出。

收稿日期: 2021-12-20; 修回日期: 2022-01-30; 录用日期: 2022-02-24

基金项目: 浙江省教育厅一般科研项目(Y202146926)、国家自然科学基金(61705055)、浙江省重点研发计划项目(2019C01G1121168)、浙江省大学生科技创新活动计划暨新苗人才计划项目(2022R407B065)

通信作者: \*zhouxf@hdu.edu.cn

## 2 基本原理

### 2.1 结构与原理介绍

图 1 为所提出的双 Lyot 滤波器结构,该滤波器由两个起偏器(POL)、两个 50/50 耦合器(OC)、两个 PC 和两段不同长度的 PMF 组成,其中  $E_{in}$  表示入射光矢量,  $E_{out}$  表示出射光矢量。入射光经过 POL1 后,成为线偏振光,被 OC1 等功率地分成两束,分别耦合进入两个支路。其中一束线偏振光经过 PC 后,偏振态与所在支路 PMF 的快慢轴存在一定夹角(理想情况下为  $45^\circ$ )。随后,进入 PMF 的线偏振光被分解为两束正交矢量模,分别在 PMF 的快轴和慢轴上传播,由于

快慢轴的有效折射率不同,这两束正交矢量模会产生与波长相关的相位差。另一束线偏振光的偏振态经由 PC 旋转后,与 PMF 的快轴或慢轴平行,此时进入 PMF 的线偏振光仅在 PMF 的一个主轴上传输,不会产生波长相关的相位差。到达 OC2 的两束光被合束,随后经过 POL2,投影到一个平面上,发生干涉。当两支路上的 PMF 长度差相对较大时(近似以  $m$  为单位),支路与支路在 OC2 处可能发生干涉,所形成的通道间隔非常小,此时通道间隔主要由 PMF 引起的相位差决定。仔细调节两个支路上的 PC,即可选择合适的 PMF 来产生波长相关的相位差,实现通道间隔的切换。

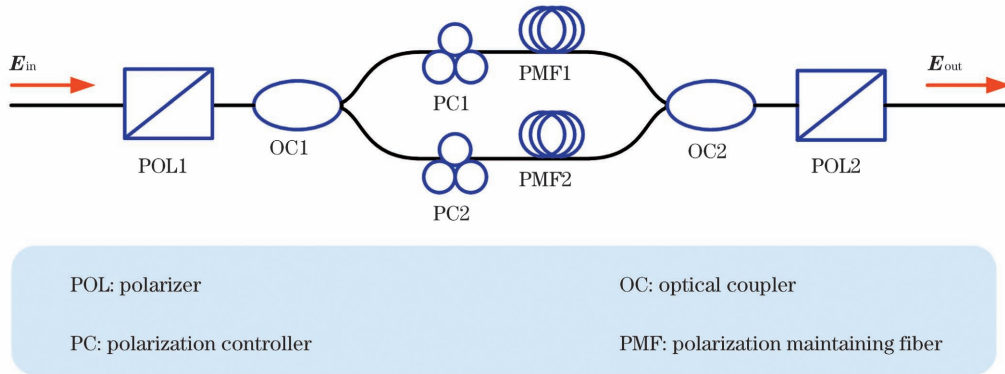


图 1 所提梳状滤波器的结构  
Fig. 1 Structure of proposed comb filter

### 2.2 理论推导

为了简化滤波器传输过程的分析,设两段 PMF 的快慢轴分别平行,定为  $x$  轴(快轴)和  $y$  轴(慢轴)。理论推导从经过第一起偏器 POL1 后的偏振光的电矢量  $E'_{in}$  开始,令起偏器与  $x$  轴的夹角为  $\theta_1$ ,  $E'_{in}$  可以表示为

$$E'_{in} = \begin{bmatrix} \cos \theta_1 \\ \sin \theta_1 \end{bmatrix}. \quad (1)$$

OC1 和 OC2 的传输矩阵<sup>[24]</sup>可近似表示为

$$T_{OC1} = \begin{bmatrix} \sqrt{1-k_1} \mathbf{I} & j\sqrt{k_1} \mathbf{I} \\ j\sqrt{k_1} \mathbf{I} & \sqrt{1-k_1} \mathbf{I} \end{bmatrix}, \quad (2)$$

$$T_{OC2} = \begin{bmatrix} \sqrt{1-k_2} \mathbf{I} & j\sqrt{k_2} \mathbf{I} \\ j\sqrt{k_2} \mathbf{I} & \sqrt{1-k_2} \mathbf{I} \end{bmatrix}, \quad (3)$$

式中:  $k_1$  和  $k_2$  分别为耦合器 OC1 和 OC2 的耦合比;  $\mathbf{I}$  为单位矩阵。PC 的琼斯矩阵<sup>[24]</sup>可以描述为

$$R_\alpha = \begin{bmatrix} \cos \alpha & \sin \alpha \\ -\sin \alpha & \cos \alpha \end{bmatrix}, \quad (4)$$

$$R_\beta = \begin{bmatrix} \cos \beta & \sin \beta \\ -\sin \beta & \cos \beta \end{bmatrix}, \quad (5)$$

式中:  $\alpha$  和  $\beta$  表示经过 PC1 和 PC2 后,光束各自偏振态相对于  $x$  轴顺时针旋转的角度。

光经过 PMF 的过程<sup>[19]</sup>可以理解为

$$J_{PMF1} = \begin{bmatrix} \exp\left(-j\frac{2\pi n_{f1}L_1}{\lambda}\right) & 0 \\ 0 & \exp\left(-j\frac{2\pi n_{s1}L_1}{\lambda}\right) \end{bmatrix}, \quad (6)$$

$$J_{PMF2} = \begin{bmatrix} \exp\left(-j\frac{2\pi n_{f2}L_2}{\lambda}\right) & 0 \\ 0 & \exp\left(-j\frac{2\pi n_{s2}L_2}{\lambda}\right) \end{bmatrix}, \quad (7)$$

式中:  $n_{f1}$  和  $n_{s1}$  为 PMF1 快慢轴的折射率;  $n_{f2}$  和  $n_{s2}$  为 PMF2 快慢轴的折射率;  $L_1$  和  $L_2$  为对应 PMF 的长度;  $\lambda$  为光波长。当 POL2 与  $x$  轴成  $\theta_2$ , 光经过 POL2 后<sup>[25]</sup>可以表述为

$$J_{POL} = \begin{bmatrix} \cos^2 \theta_2 & \frac{1}{2} \sin(2\theta_2) \\ \frac{1}{2} \sin(2\theta_2) & \cos^2 \theta_2 \end{bmatrix}. \quad (8)$$

可以通过以下矩阵分析滤波器的输出特性:

$$\begin{bmatrix} E_{out} \\ \mathbf{0} \end{bmatrix} = \begin{bmatrix} J_{POL} & \mathbf{0} \\ \mathbf{0} & \mathbf{0} \end{bmatrix} \cdot T_{OC2} \begin{bmatrix} J_{PMF1} R_\alpha & \mathbf{0} \\ \mathbf{0} & J_{PMF2} R_\beta \end{bmatrix} T_{OC1} \begin{bmatrix} E'_{in} \\ \mathbf{0} \end{bmatrix}, \quad (9)$$

式中:  $\mathbf{0}$  为零矩阵。

由此可得滤波器的传输函数为

$$T = \left| \frac{\mathbf{E}_{\text{out}}}{\mathbf{E}'_{\text{in}}} \right|^2 = (1 - k_1)(1 - k_2) \left\{ \cos^2(\theta_1 - \alpha) \cos^2\theta_2 + \frac{1}{2} \sin(2\theta_2) \sin[2(\theta_1 - \alpha)] \cos(\varphi_1 - \varphi_3) + \sin^2(\theta_1 - \alpha) \sin^2\theta_2 \right\} + k_1 k_2 \left\{ \cos^2(\theta_1 - \beta) \cos^2\theta_2 + \frac{1}{2} \sin(2\theta_2) \sin[2(\theta_1 - \beta)] \cos(\varphi_2 - \varphi_4) + \sin^2(\theta_1 - \beta) \sin^2\theta_2 \right\} - 2\sqrt{k_1 k_2 (1 - k_1)(1 - k_2)} \times [\cos^2\theta_2 \cos(\theta_1 - \alpha) \cos(\theta_1 - \beta) \cos(\varphi_1 - \varphi_2) + \frac{1}{2} \sin(2\theta_2) \cos(\theta_1 - \alpha) \sin(\theta_1 - \beta) \cos(\varphi_1 - \varphi_4) + \frac{1}{2} \sin(2\theta_2) \sin(\theta_1 - \alpha) \cos(\theta_1 - \beta) \cos(\varphi_2 - \varphi_3) + \sin^2\theta_2 \sin(\theta_1 - \alpha) \sin(\theta_1 - \beta) \cos(\varphi_3 - \varphi_4)], \quad (10)$$

式中： $\varphi_1 = \frac{2\pi n_{f1} L_1}{\lambda}$ ,  $\varphi_2 = \frac{2\pi n_{f2} L_2}{\lambda}$ ,  $\varphi_3 = \frac{2\pi n_{s1} L_1}{\lambda}$ ,  $\varphi_4 = \frac{2\pi n_{s2} L_2}{\lambda}$ , 分别表示偏振光在 PMF1 和 PMF2 快慢轴上传输时发生的相位变化； $\theta_1 - \alpha$  和  $\theta_1 - \beta$  为相应支路上偏振光与  $x$  轴的夹角。式(10)的第一、二项所包含的相位信息  $\varphi_1 - \varphi_3$  和  $\varphi_2 - \varphi_4$ , 分别表示由 PMF1 和 PMF2 引起的波长相关相位差。根据边界条件, 相位差  $\Delta\varphi = 2\pi m$  ( $m = 0, 1, 2, \dots$ ), 由 PMF1、PMF2 引起的通道间隔依次为

$$\Delta\lambda_1 = \frac{\lambda^2}{B_{\text{PMF1}} L_1}, \quad (11)$$

$$\Delta\lambda_2 = \frac{\lambda^2}{B_{\text{PMF2}} L_2}, \quad (12)$$

式中： $B_{\text{PMF1}} = |n_{f1} - n_{s1}|$ ,  $B_{\text{PMF2}} = |n_{f2} - n_{s2}|$ , 分别表示 PMF1 和 PMF2 的双折射率。双折射率的量级为  $10^{-4}$ , 因此  $\Delta\lambda_1$  和  $\Delta\lambda_2$  的量级为  $10^{-10} \sim 10^{-9}$  m。式(10)的最后一项包含相位信息  $\varphi_1 - \varphi_2$ ,  $\varphi_1 - \varphi_4$ ,  $\varphi_2 - \varphi_3$  和  $\varphi_3 - \varphi_4$ , 它们由两段 PMF 的长度差引起。当 PMF 长度差近似以 m 为单位且输入光为非相干光时, 此项可视为直流分量。值得注意的是, 当输入光为相干光时, 此项显示了滤波器所能形成的小干涉条纹间距, 量级为  $10^{-12}$  m。小干涉条纹无法被光谱仪观测, 其在两种对应通道间隔下所能产生的包络周期与对应通道间隔长度相同, 不会对通道间隔产生影响。

### 3 仿真与分析

剔除式(10)中的直流分量, 保留波长相关项:

$$T = \frac{1}{2} (1 - k_1)(1 - k_2) \sin(2\theta_2) \sin[2(\theta_1 - \alpha)] \cdot \cos(\varphi_1 - \varphi_3) + \frac{1}{2} k_1 k_2 \sin(2\theta_2) \sin[2(\theta_1 - \beta)] \cdot \cos(\varphi_2 - \varphi_4). \quad (13)$$

当  $\theta_2 \neq C\pi$  ( $C = 0, 1, 2, \dots$ ) 时, 调节 PC, 使  $\theta_1 - \alpha$

和  $\theta_1 - \beta$  中的一项为  $\frac{\pi}{2}$  的整数倍, 而另一项不是。换言之, 使滤波器中一条支路上的偏振光与该支路上的 PMF 主轴之一平行, 而另一路不平行。此时, 仅剩一个包含相位信息的项, 即实现了通道间隔的切换。传输矩阵理论的推导结果与原理分析完全一致。设  $k_1 = k_2 = 0.5$ ,  $B_{\text{PMF1}} = B_{\text{PMF2}} = 5.1 \times 10^{-4}$ ,  $L_1 = 7.2$  m,  $L_2 = 13.5$  m, 绘制滤波器的仿真透射谱, 模拟实现通道间隔切换的情况。固定 PC1, 使  $\theta_1 - \alpha = \frac{\pi}{4}$ , 改变 PC2, 即改变  $\theta_1 - \beta$ , 如图 2(a) 所示。

当  $\theta_1 - \beta = C'\frac{\pi}{2}$  ( $C' = 0, 1, 2, \dots$ ) 时, 梳状谱形状规则, 通道间隔为 0.65 nm, 此时的通道间隔由 PMF1 提供。固定  $\theta_1 - \beta = \frac{\pi}{4}$ , 改变  $\theta_1 - \alpha$ , 当  $\theta_1 - \alpha$  为  $\frac{\pi}{2}$  的倍数时, 可得到由 PMF2 提供的 0.35 nm 的稳定通道间隔, 如图 2(b) 所示。仿真结果与理论分析计算相吻合。

改变两并联 PMFs 的特性, 使两者的双折射率依次为  $B_{\text{PMF1}} = 4.0 \times 10^{-4}$ ,  $B_{\text{PMF2}} = 5.1 \times 10^{-4}$ , 长度分别为  $L_1 = 6.6$  m,  $L_2 = 10$  m。当  $\theta_1 - \alpha$  和  $\theta_1 - \beta$  分别为  $\pi/4$  和 0 时, 滤波器的通道间隔为 0.91 nm; 当  $\theta_1 - \alpha$  和  $\theta_1 - \beta$  分别为 0 和  $\pi/4$  时, 滤波器通道间隔为 0.47 nm, 与式(11)、(12)的计算结果吻合, 如图 3 所示。结果表明, 更换不同的 PMF 可以得到新的通道间隔可切换组合。

调节 PC 除了可实现通道间隔切换外, 还可实现消光比的调谐。以上述 0.91 nm 通道间隔的情况 ( $\theta_1 - \beta = 0$ ) 为例, 调节 PC1 (即调节  $\theta_1 - \alpha$ ), 当  $0 \leq \theta_1 - \alpha \leq \frac{\pi}{2}$  时, 随着  $\theta_1 - \alpha$  的增大, 透射谱振幅增大, 如图 4(a) 所示。实际上, 根据式(13), 滤波器透射谱的消光比随着  $\theta_1 - \alpha$  的增大呈正弦周期变化, 如图 4(b) 所示。



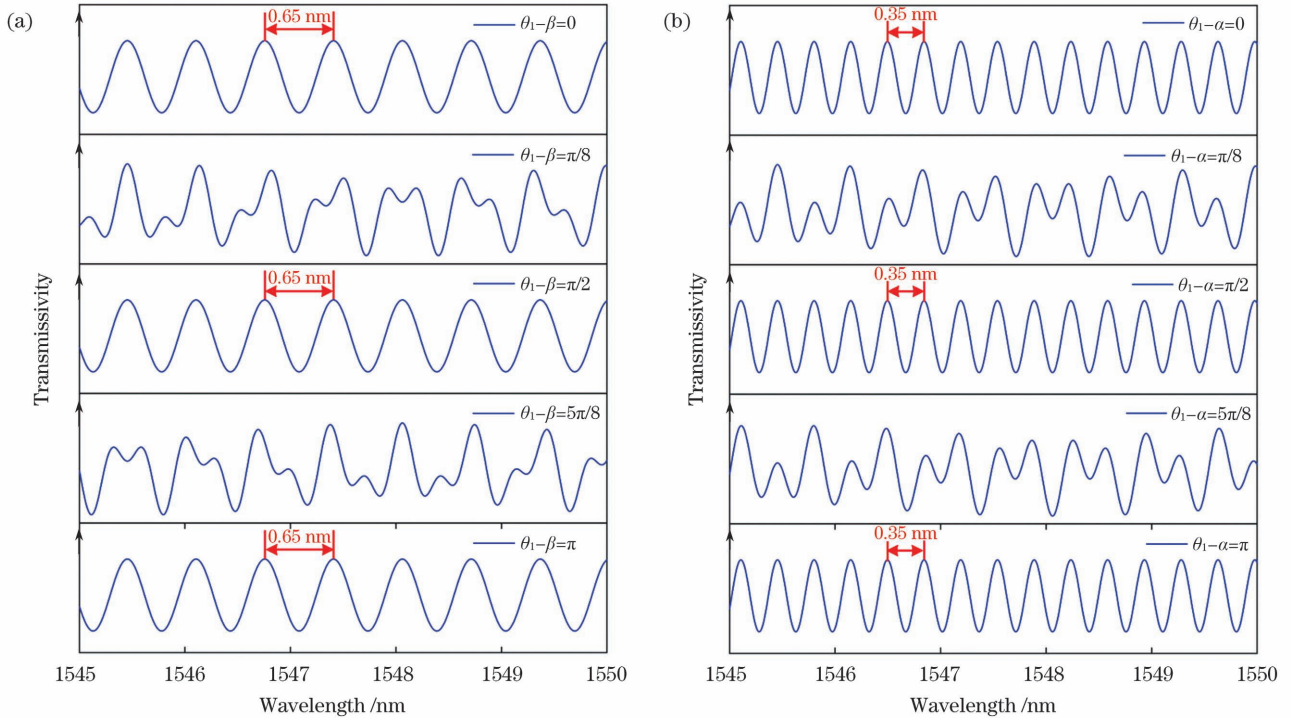


图 2 滤波器的仿真透射谱。(a)  $\theta_1 - \alpha = \frac{\pi}{4}$  时调节 PC2; (b)  $\theta_1 - \beta = \frac{\pi}{4}$  时调节 PC1

Fig. 2 Simulated transmission spectra of filter. (a) Rotating PC2 when  $\theta_1 - \alpha = \frac{\pi}{4}$ ; (b) rotating PC1 when  $\theta_1 - \beta = \frac{\pi}{4}$

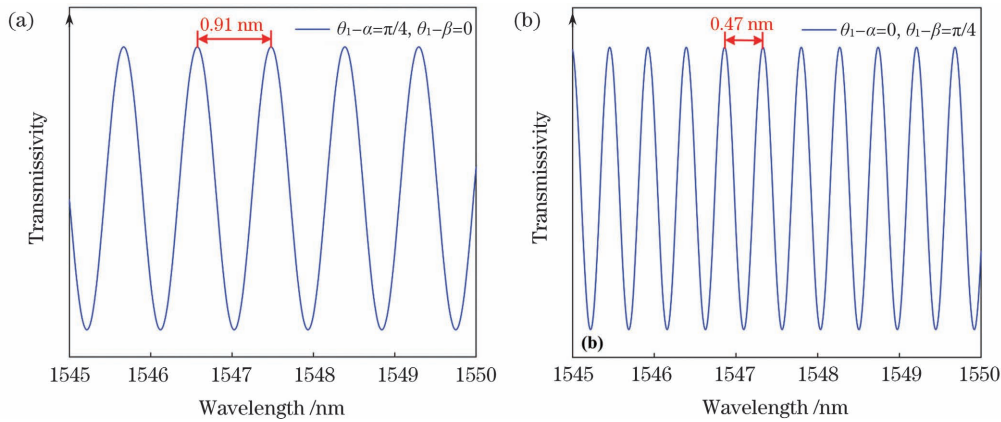


图 3 新的通道间隔组合。(a)通道间隔由 PMF1 决定; (b)通道间隔由 PMF2 决定

Fig. 3 New channel interval combinations. (a) Channel interval determined by PMF1; (b) channel interval determined by PMF2

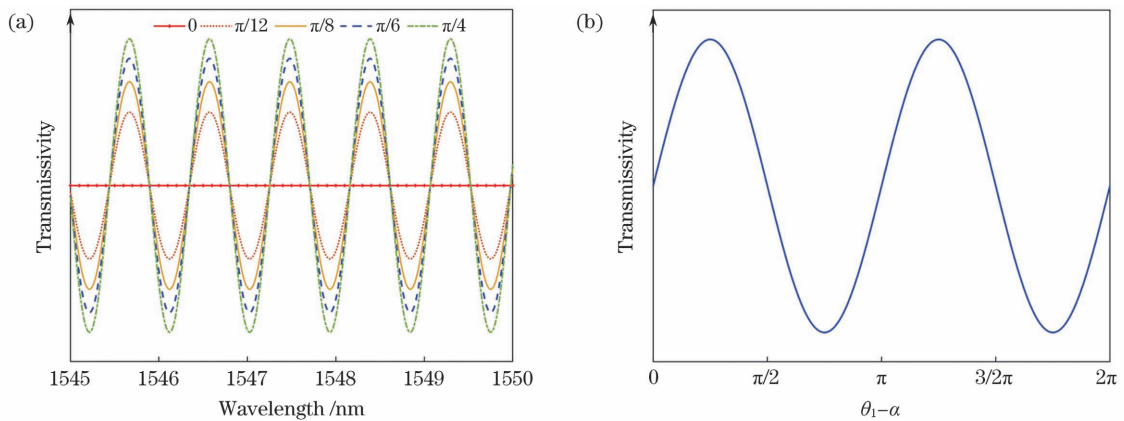


图 4 在固定 PC2、调节 PC1 时的消光比变化。(a)PC1 对透射谱的影响; (b)PC1 对透射谱振幅的影响

Fig. 4 Fluctuation of extinction ratio when PC2 is fixed and PC1 is adjusted. (a) Effect of PC1 on transmission spectrum; (b) effect of PC1 on amplitude of transmission spectrum

观察式(13),除 PC 外,  $x$  轴与 POL2 的夹角  $\theta_2$  对滤波器消光比同样存在一定影响。固定 PC, 当  $\theta_2 = \frac{\pi}{4} + C''\pi$  ( $C''=0,1,2,\dots$ ) 时, 滤波器的消光比最大。然而在实际的应用中,  $\theta_2$  的大小不可调节, 因此得到的消光比无法达到理论上的最大值。可通过在 POL2 前增加一个 PC 的方式解决这个问题, PC+POL2 的组合相当于一个角度可旋转的起偏器,  $x$  轴与可旋转起偏器之间的夹角可以理解为  $\theta_2' = \gamma + \theta_2$ , 其中  $\gamma$  为新增 PC 旋转的角度。

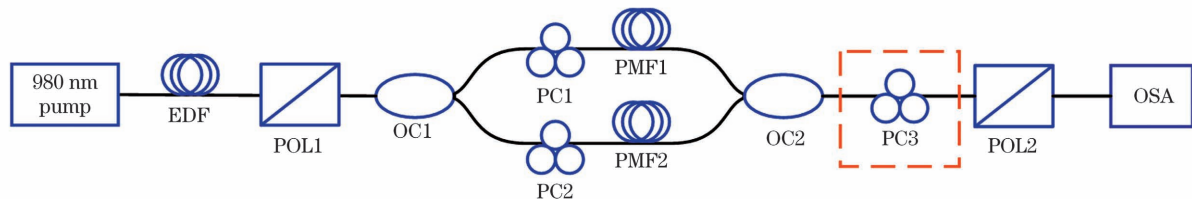
## 4 实验与讨论

### 4.1 双 Lyot 滤波器的传输特性测量

搭建的实验装置如图 5 所示。装置中泵浦源的输出波长为 980 nm, 掺铒光纤 (EDF) 的长度为 5 m, 用于提供自发辐射谱; 两个耦合器的耦合比均为 50:50, 用于均分光功率; 两段 PMF 的双折射率均为  $5.1 \times 10^{-4}$ , 长度依次为 7.2 m 和 13.5 m, 用于产生两种不

同的通道间隔; 光谱分析仪 (OSA) 的分辨率为 0.02 nm, 用于观测滤波器的透射谱。当泵浦功率为 150 mW 时, 滤波器在有/无 PC3 时, 观察到的振幅最大的光谱如图 6 所示。

其中, 0.65 nm 到 0.34 nm 的通道间隔切换可通过调节 PC1 和 PC2 来实现, 通道间隔的表现与仿真结果图 2 一致。此外, 增加了 PC3 的实验装置表现出了更好的消光比, 证实了前文的分析结果。值得注意的是, 当实验中的输出光谱对应两个通道间隔的混合时, 仅通过调节 PC3 也可以选出其中一种通道间隔。这是因为理论分析讨论的是两段 PMF 的快慢轴分别平行的理想情况, 实际在没有进行精确对准的情况下, 两段 PMF 的主轴之间存在一定夹角。当 PC+POL2 组合的透光角度与其中一段 PMF 的某一个主轴平行时, 其效果与调节 PC1 或 PC2 使其与对应 PMF 的某个主轴平行相同。因此在实际使用过程中, 增设了 PC3 的滤波结构具有更强的可调性, 不论是调节 PC1 和 PC2 还是调节 PC3 均可实现通道间隔的切换和消光比的调谐。



WDM: wavelength division multiplexer  
PC: polarizer

POL: polarizer  
PMF: polarization maintaining fiber

OC: optical coupler  
OSA: optical spectrum analyzer

图 5 改进结构的滤波器实验装置

Fig. 5 Experimental setup of filter with improved structure

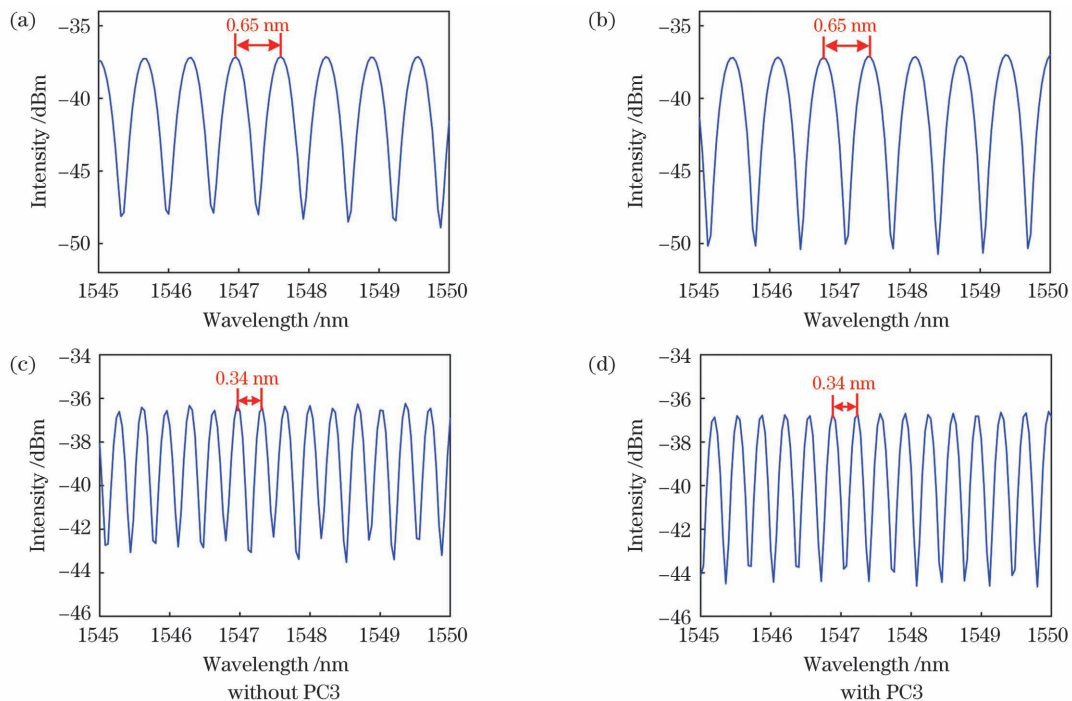


图 6 实验获得的最大振幅光谱图。(a)(b)通道间隔为 0.65 nm; (c)(d)通道间隔为 0.34 nm

Fig. 6 Spectra with maximum amplitude obtained in experiment. (a)(b) Channel interval is 0.65 nm; (c)(d) channel interval is 0.34 nm

### 4.2 基于双 Lyot 滤波器的激光器应用

为了验证双 Lyot 滤波器在激光器应用中可实现通道间隔切换,搭建了激光器实验装置,如图 7 所示。其中,高非线性光纤(HNLF)长度为 105 m,OC3 的耦合比为 10:90,其余器件参数与 4.1 节相同编号的器件相同。在中心波长为 980 nm 的泵浦源的激励下,由 EDF 产生的自发辐射光被隔离器约束,逆时针方向传输,经过双 Lyot 滤波器后,依次通过 HNLF、OC3 的 90% 端口和波分复用器(WDM),反复循环谐振产生稳定的多波长激光,并在 OC3 的 10% 端口输出。其中,HNLF 用于增强非线性效应,促进四波混频的产生,有效降低室温下 EDF 的均匀展宽效应带来的剧烈模式竞争影响,实现功率均衡。

激光器的两种输出光谱可通过调节 PC 来实现切换,测量结果如图 8 所示。图 8(a)为泵浦功率为 250 mW 时,通道间隔为 0.65 nm 的多波长输出结果;图 8(b)为泵浦功率为 356 mW 时,通道间隔为 0.34 nm 的多波长输出结果。两种激光输出的通道间隔与滤波器透射谱通道间隔的实测结果一致。实验结果显示,在相同波数和接近的输出波长光功率下,小通道间隔的损耗要高于大通道间隔。这是因为实验使用的 13.5 m 长的 PMF 的损耗较大;工作在小通道间隔下的激光器的内部模式竞争更剧烈,需要较强的光功率来引发足够强的非线性效应。此外,由于光在进入第一、第二偏振控制器前的偏振态是确定的,通道间隔切换的可重复性较强。

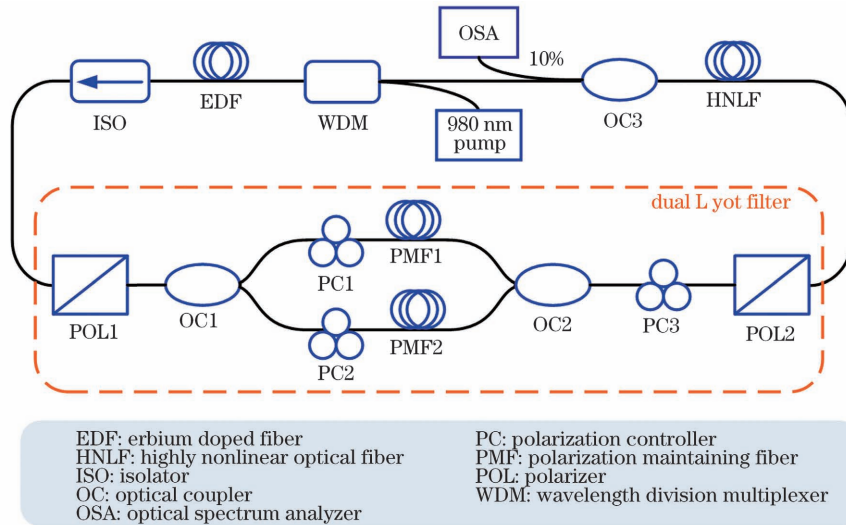


图 7 基于双 Lyot 滤波器的多波长光纤激光器实验装置

Fig. 7 Experimental setup of MWFL based on dual Lyot filter

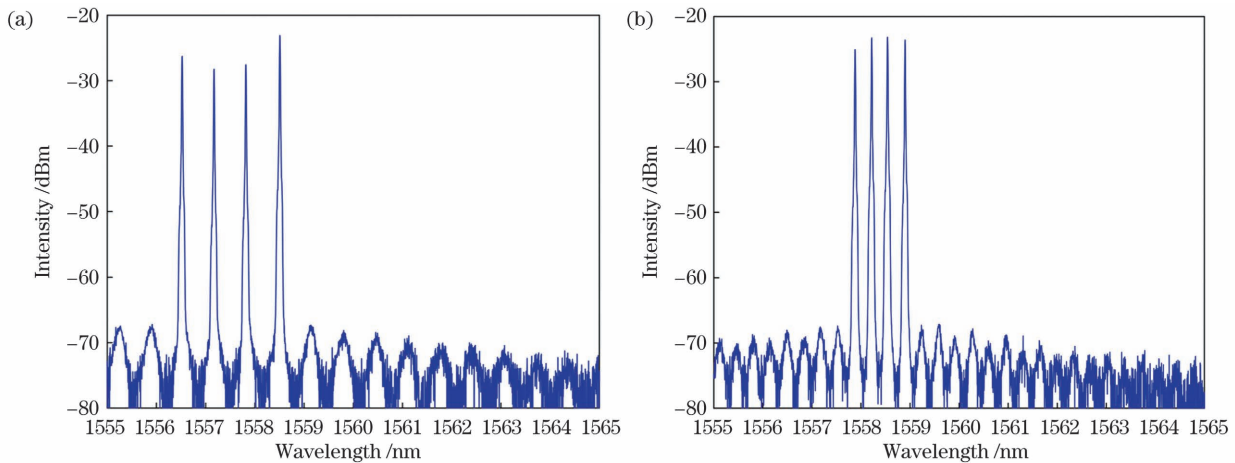


图 8 多波长输出光谱图。(a)通道间隔为 0.65 nm; (b)通道间隔为 0.34 nm

Fig. 8 Multi-wavelength output spectra. (a) Channel interval is 0.65 nm; (b) channel interval is 0.34 nm

## 5 结 论

通过原理分析、理论推导和实验测试,验证了一种通道间隔可切换的全光纤梳状滤波器。该滤波器的通道间隔由双 Lyot 滤波器中并联的 PMFs 决定,可通过调节 PCs 切换通道间隔并调节消光比。在第二起偏

器前增加一个 PC 可以进一步提高滤波器的可调性。针对不同场景的现实需要,通过灵活更换 PMFs,可得到新的通道间隔可切换组合。最后,将设计的滤波器应用于多波长光纤激光器中,实现了激光输出的通道间隔切换,进一步证明了滤波器的实用性。值得注意的是,在应用中,滤波器的两段 PMFs 长度差应以 m



为单位。此外,由于光路中偏振态观测困难,较难实现通道间隔非常接近的波长切换。不过,对于通道间隔很接近的情况,双 Lyot 滤波器更适合用作高灵敏度传感器的部件(利用游标效应,放大波长漂移),而不是作为通道间隔可切换的 MWFL 的波长选择元件。总之,这种新型的通道间隔可切换滤波器,在多波长光纤激光器、密集波分复用光网络和光纤传感器中均有不错的应用前景。

### 参 考 文 献

- [1] 李恒文, 江阳, 徐静, 等. 基于光纤参量环形镜的光毫米波副载波产生[J]. 光学学报, 2012, 32(10): 1006005.  
Li H W, Jiang Y, Xu J, et al. Optical millimeter-wave sub-carrier generation based on optical parametric loop mirror[J]. Acta Optica Sinica, 2012, 32(10): 1006005.
- [2] 石暖暖, 谷一英, 胡晶晶, 等. 基于 Sagnac 环可调谐光梳状滤波器特性研究[J]. 光学学报, 2014, 34(3): 0306001.  
Shi N N, Gu Y Y, Hu J J, et al. Study of the tunable optical comb filter based on Sagnac interferometer loop[J]. Acta Optica Sinica, 2014, 34(3): 0306001.
- [3] Liu X D, Lou S Q, Tang Z J, et al. Tunable and switchable triple-wavelength ytterbium-doped fiber ring laser based on Sagnac interferometer with a polarization-maintaining photonic crystal fiber [J]. Optics & Laser Technology, 2020, 122: 105848.
- [4] Ozgören K, Ilday F O. All-fiber all-normal dispersion laser with a fiber-based Lyot filter[J]. Optics Letters, 2010, 35(8): 1296-1298.
- [5] Sugavanam S, Yan Z, Kamynin V, et al. Multiwavelength generation in a random distributed feedback fiber laser using an all fiber Lyot filter[J]. Optics Express, 2014, 22(3): 2839-2844.
- [6] 林彦吕, 黄梓楠, 黄千千, 等. 基于 Lyot 滤波器的脉冲态可切换掺镱光纤激光器[J]. 中国激光, 2021, 48(19): 1901004.  
Lin Y L, Huang Z N, Huang Q Q, et al. Pulse state switchable ytterbium-doped fiber laser based on Lyot filter [J]. Chinese Journal of Lasers, 2021, 48(19): 1901004.
- [7] Peng W J, Yan F P, Li Q, et al. Tunable self-seeded multiwavelength Brillouin-erbium fiber laser using an in-line two-taper Mach-Zehnder interferometer [J]. Optics & Laser Technology, 2013, 45: 348-351.
- [8] 耿健, 朱晓军, 章国安, 等. 基于光纤布拉格光栅拉锥的带宽可调微光纤马赫-曾德尔干涉仪[J]. 光学学报, 2019, 39(3): 0306004.  
Geng J, Zhu X J, Zhang G A, et al. Bandwidth tunable microfiber-assisted mach-zehnder interferometer based on tapered-drawing fiber bragg grating [J]. Acta Optica Sinica, 2019, 39(3): 0306004.
- [9] Sun X M, Zhou L J, Xie J Y, et al. Tunable silicon Fabry-Perot comb filters formed by Sagnac loop mirrors[J]. Optics Letters, 2013, 38(4): 567-569.
- [10] 盛文娟, 董壮志, 杨宁, 等. 基于集成移动窗口的可调谐滤波器温度补偿研究[J]. 光学学报, 2021, 41(23): 2306005.  
Sheng W J, Dong Z Z, Yang N, et al. Temperature compensation of tunable filter based on integrated moving window[J]. Acta Optica Sinica, 2021, 41(23): 2306005.
- [11] 田鑫, 赵晓帆, 王蒙. 基于倾斜 FBG 的光纤受激布里渊散射抑制[J]. 光学学报, 2020, 40(17): 1706001.  
Tian X, Zhao X F, Wang M, et al. Suppression of stimulated Brillouin scattering in fiber using the tilted fiber bragg grating [J]. Acta Optica Sinica, 2020, 40(17): 1706001.
- [12] Zhao Q, Pei L, Tang M, et al. Switchable multi-wavelength erbium-doped fiber laser based on core-offset structure and four-wave-mixing effect [J]. Optical Fiber Technology, 2020, 54: 102111.
- [13] Yu F D, Xue P, Zheng J. Study of a large lateral core-offset in-line fiber modal interferometer for refractive index sensing [J]. Optical Fiber Technology, 2019, 47: 107-112.
- [14] 廖莎莎, 张甜甜, 刘继伟, 等. 低纹波因数、高形状因子的片上光学平顶滤波器[J]. 光学学报, 2021, 41(24): 2413001.  
Liao S S, Zhang T T, Liu J W, et al. On-chip optical flat-top filter with low ripple factor and high shape factor [J]. Acta Optica Sinica, 2021, 41(24): 2413001.
- [15] Cai X, Luo J, Fu H Y, et al. Temperature measurement using a multi-wavelength fiber ring laser based on a hybrid gain medium and Sagnac interferometer [J]. Optics Express, 2020, 28(26): 39933-39943.
- [16] 田鑫, 王蒙, 王泽锋. 基于倾斜光纤 Bragg 光栅的受激布里渊散射滤波器[J]. 光学学报, 2020, 40(10): 1006002.  
Tian X, Wang M, Wang Z F. Stimulated Brillouin scattering filters based on tilted fiber Bragg gratings [J]. Acta Optica Sinica, 2020, 40(10): 1006002.
- [17] 胡琪浩, 赵晓帆, 田鑫, 等. 基于长周期光纤光栅的受激拉曼散射滤波器[J]. 光学学报, 2021, 41(18): 1806003.  
Hu Q H, Zhao X F, Tian X, et al. Stimulated Raman scattering filters based on long period fiber gratings [J]. Acta Optica Sinica, 2021, 41(18): 1806003.
- [18] Lü Y, Lou S Q, Tang Z J, et al. Tunable C-band and L-band multi-wavelength erbium-doped fiber ring laser based on a triple-core photonic crystal fiber with polarization-dependent loss [J]. Optics & Laser Technology, 2020, 128: 106269.
- [19] Luo A P, Luo Z C, Xu W C. Tunable and switchable multi-wavelength erbium-doped fiber ring laser based on a modified dual-pass Mach-Zehnder interferometer [J]. Optics Letters, 2009, 34(14): 2135-2137.
- [20] Wang J, Zheng K, Peng J, et al. Theory and experiment of a fiber loop mirror filter of two-stage polarization-maintaining fibers and polarization controllers for multiwavelength fiber ring laser [J]. Optics Express, 2009, 17(13): 10573-10583.
- [21] Wang W, Meng H Y, Wu X W, et al. Three channel-spacing switchable multiwavelength fiber laser with two segments of polarization-maintaining fiber [J]. IEEE Photonics Technology Letters, 2012, 24(6): 470-472.
- [22] Zhao Q, Pei L, Zheng J J, et al. Tunable and interval-adjustable multi-wavelength erbium-doped fiber laser based on cascaded filters with the assistance of NPR [J]. Optics & Laser Technology, 2020, 131: 106387.
- [23] He W, Shanguan C M, Zhu L Q, et al. Tunable and stable multi-wavelength erbium-doped fiber laser based on a double Sagnac comb filter with polarization-maintaining fibers [J]. Optik, 2017, 137: 254-261.
- [24] 崔文翔, 周雪芳, 胡森, 等. 双 Sagnac 环滤波器的传输特性分析和实验研究[J]. 中国激光, 2022, 49(4): 0406006.  
Cui W X, Zhou X F, Hu M, et al. Analysis and experimental study on transmission characteristics of double Sagnac loop filter [J]. Chinese Journal of Lasers, 2022, 49(4): 0406006.
- [25] Li Y H, Lou C Y, Wu J, et al. Novel method to simultaneously compress pulses and suppress supermode noise in actively mode-locked fiber ring laser [J]. IEEE Photonics Technology Letters, 1998, 10(9): 1250-1252.

# Structural Design and Performance Analysis of Dual Lyot Filter with Switchable Channel Interval

Xin Lingyi<sup>1</sup>, Zhou Xuefang<sup>1\*</sup>, Bi Meihua<sup>1</sup>, Yang Guowei<sup>1</sup>, Hu Miao<sup>1</sup>,  
Li Haozhen<sup>1</sup>, Wang Tianshu<sup>2</sup>

<sup>1</sup>*School of Communication Engineering, Hangzhou Dianzi University, Hangzhou 310018, Zhejiang, China;*

<sup>2</sup>*Institute of Space Optoelectronics Technology, Changchun University of Science and Technology, Changchun 130022, Jilin, China*

## Abstract

**Objective** Fiber comb filters are widely concerned because of simple structure, low cost, strong stability, and strong compatibility with optical fiber communication systems. A common application scenario for fiber comb filters involves multiwavelength fiber lasers ( MWFLs ). Generally, an all-fiber comb filter is fixed with a constant channel interval that is challenging to meet the needs of tunability in some practical uses. In previous research, our team has conducted detailed theoretical studies and transmission characteristics tests on a double Sagnac loop and experimentally verified its viability in channel interval switching when used in MWFL. In this research, we unravel the double Sagnac loop and transform it into a novel dual Lyot filter based on parallel polarization-maintaining fibers. The findings of theoretical analysis and experimental tests demonstrate that the channel interval is switchable and the extinction ratio is tunable with the polarization controller's adjustment. The MWFL based on the dual Lyot filter is capable of generating a multiwavelength output with two various channel intervals. This research may provide some references for scholars who engage in the study of MWFL with high flexibility.

**Methods** First, the designed dual Lyot filter's transmission function is derived based on the theoretical analysis and the transfer matrix theory. Then, the transmission spectrum is simulated using the Matlab software. The channel interval switch function is confirmed from a theoretical perspective. By replacing the polarization-maintaining fibers ( PMFs ), various wavelength interval combinations can be accessible, further confirming the filtering structure's flexibility in obtaining channel interval switching. After that, the impact of the polarization controller ( PC ) before PMF on the extinction ratio ( ER ) of the transmission spectrum is discussed. Furthermore, a PC is added to the proposed filter to optimize the filter's ER performance and tunability. Moreover, to confirm the theoretical conclusion, the experimental measurement of the transmission spectrum and the performance comparison of the filter before and after the optimization are conducted. Finally, a multiwavelength fiber laser based on the optimized filter is experimentally demonstrated, and its channel interval switch ability is confirmed in the laser system.

**Results and Discussions** The dual Lyot filter's transmission function ( Eq. 10 ) is derived using a transmission matrix. The filter's simulation transmission spectrum is drawn to simulate channel interval switching ( Fig. 2 ) with the following parameters: the coupling coefficient  $k_1 = k_2 = 0.5$ , the two PMFs' birefringence  $B_{\text{PMF1}} = B_{\text{PMF2}} = 5.1 \times 10^{-4}$ , and the PMFs' lengths  $L_1 = 7.2$  m and  $L_2 = 13.5$  m. When the polarized light's angle to the fast axis of PMF2 is a multiple of  $\pi/2$ , the filter's channel interval is produced by PMF1 with a length of 0.65 nm. Similarly, when the polarized light's angle to the fast axis of PMF1 is a multiple of  $\pi/2$ , the channel interval is 0.35 nm produced by PMF2. The simulation findings are consistent with the theoretical computation. Changing the characteristics of two parallel PMFs with the following parameters:  $B_{\text{PMF1}} = 4.0 \times 10^{-4}$ ,  $B_{\text{PMF2}} = 5.1 \times 10^{-4}$ ,  $L_1 = 6.6$  m, and  $L_2 = 10$  m. Two new channel intervals of 0.91 nm and 0.47 nm can be obtained ( Fig. 3 ). In addition to the switching of channel interval, the PC can be adjusted for the ER turning. The filter transmission spectrum's ER varies sinusoidally as the polarized light's angle to the PMFs' fast axis (  $x$ -axis ) increases ( Fig. 4 ). In the transmission characteristic experiment, the same PMFs as Fig. 2 are taken to compare the filter's maximum amplitude before and after optimization ( Fig. 6 ). The transmission spectra with the channel intervals of 0.65 nm and 0.34 nm obtained agree with the simulation findings. The optimized filter demonstrates a better ER and tunability. An experiment is performed to confirm that the dual Lyot filter allows channel interval switching in laser applications ( Fig. 7 ). In the experiment, the highly nonlinear fiber is 105 m long, the coupling ratio of OC3 is 10:90, and the rest device parameters are the same as those for testing transmission characteristics. Modifying the PC gives two multiwavelength laser outputs with channel intervals of 0.65 nm and 0.34 nm, respectively ( Fig. 8 ). The two laser outputs' channel intervals are consistent with the channel interval measured by the filter transmission spectrum.

**Conclusions** In this research, an all-fiber comb filter with a switchable channel interval is proposed based on theoretical derivation and experimental verification. The filter's channel interval is determined by the PMFs connected in parallel in



the dual Lyot filter. By replacing the PMFs, various wavelength interval combinations are accessible, meeting the requirements of diverse application situations. Careful adjustment of the PC allows the channel interval switching and the ER's tuning. The experimental findings show an optimized turnability by adding a PC to the filter. Moreover, the filter's practicality is further shown using the designed filter with a multiwavelength fiber laser. The two PMFs' length difference in the filter is preferable in the unit of meter. Additionally, it is challenging to switch the channel intervals if they are very close, because of the challenges of observing the polarization state in the optical path. However, for the close channel intervals, the filter under this structure is better to be used as a component of a highly sensitive sensor with a vernier effect rather than a wavelength selection element of MWFL with a flexible channel interval. In conclusion, the dual Lyot filter has considerable uses in MWFLs, dense wavelength division multiplexing optical networks, and fiber optic sensors.

**Key words** fiber optics; comb filter; transfer matrix; Lyot filter; switchable channel interval